Structural basis of long-range transcription-translation coupling

Chengyuan Wang[1--2,*], Vadim Molodtsov[1,3-4,*], Jason T. Kaelber[5], Gregor Blaha[6], and Richard H. Ebright[1,**]

[1]Waksman Institute and Department of Chemistry and Chemical Biology, Rutgers University, Piscataway, NJ 08854, USA.

[2]Shanghai Institute of Immunity and Infection, Chinese Academy of Sciences, Shanghai 200032, China.

[3]Research Institute of Molecular and Cellular Medicine RUDN, Moscow 115093, Russia.

[4]Skolkovo Institute of Science and Technology, Moscow 121205, Russia.

[5]Rutgers CryoEM and Nanoimaging Facility and Institute for Quantitative Biomedicine, Rutgers University, Piscataway, NJ 08854, USA.

[6]Department of Biochemistry, University of California, Riverside, CA 92521, USA.

*Contributed equally.

**Correspondence to: ebright@waksman.rutgers.edu

Short title:

Long-range transcription-translation coupling.

Abstract

Structures recently have been reported of molecular assemblies that mediate transcription-translation coupling in *Escherichia coli*. In these molecular assemblies, termed "coupled transcription-translation complexes" or "TTC-B", RNA polymerase (RNAP) interacts directly with the ribosome, the transcription elongation factor NusG or its paralog RfaH forms a bridge between RNAP and ribosome, and the transcription elongation factor NusA optionally forms a second bridge between RNAP and ribosome. Here, we have determined structures of coupled transcription-translation complexes having mRNA spacers between RNAP and ribosome longer than the maximum-length mRNA spacer compatible with formation of TTC-B. The results define a new class of coupled transcription-translation complex, termed "TTC-LC," where "LC" denotes "long-range coupling." TTC-LC differs from TTC-B by a ~60º rotation and ~70 Å translation of RNAP relative to ribosome, resulting in loss of direct interactions between RNAP and ribosome and creation of a ~70 Å gap between RNAP and ribosome. TTC-LC accommodates long mRNA spacers by looping out mRNA from the gap between RNAP and ribosome. We propose that TTC-LC is an intermediate in assembling and disassembling TTC-B, mediating pre-TTC-B transcription-translation coupling before a ribosome catches up to RNAP, and mediating post-TTC-B transcription-translation coupling after a ribosome stops moving and RNAP continues moving.

Introduction

Bacterial transcription and translation occur in the same cellular compartment[1-2], occur at the same time[1-2], and, in many cases, are functionally coordinated and physically coupled processes, in which the rate of transcription by the first molecule of RNA polymerase (RNAP) synthesizing an mRNA is coordinated with the rate of translation by the first ribosome translating the mRNA[2-14]. Transcription-translation coupling increases transcription elongation rates, suppresses transcription pausing, suppresses transcription termination, increases translation elongation rates, suppresses translation pausing, and plays roles in regulation of gene expression[3-24]. In the bacterium *Escherichia coli*, the physical coupling of transcription and translation is mediated by the transcription elongation factor NusG

and its paralog RfaH[4-14,25-29]. NusG is a general coupling factor that couples transcription and translation at most genes in *E. coli*[4-14,25-29], and RfaH is a specialized, regulon-specific coupling factor that couples transcription and translation at a small number of genes in *E. coli* that contain a DNA sequence, termed an *ops* site, required for loading RfaH onto RNAP[5-7,10-13,25-29]. NusG and RfaH each consists of an N-terminal domain (NusG-N or RfaH-N) that interacts with RNAP, a C-terminal domain (NusG-C or RfaH-C) that interacts with ribosomal protein S10, and an interdomain linker[4-5,7-14,25-29]. *E. coli* transcription-translation coupling is further mediated by a second transcription elongation factor, NusA[30].

Structures of NusG- and RfaH-containing *E. coli* transcription-translation complexes (TTCs) recently have been reported[31-34]. Two distinct structural classes of TTCs have been described: (i) "collided TTCs", also referred to as "TTC-A", which have structural features that suggest they are translationally inactive, or only partly, active products of collision between a ribosome and RNAP[31-34]; and (ii) "coupled TTCs", also referred to as "TTC-B", which have structural features that suggest that they are the translationally active complexes that mediate functional transcription-translation coupling[32-34]. Structures of NusG- and RfaH-coupled TTC-B are superimposable, differing only in that NusG-coupled TTC-B shows greater conformational heterogeneity in the orientation of RNAP relative to the ribosome than RfaH-coupled TTCs (Fig. 1)[34]. In both NusG- and RfaH-coupled TTC-B, the coupling factor NusG or RfaH bridges RNAP and the ribosome, with NusG-N or RfaH-N interacting with RNAP, and with NusG-C or RfaH-C simultaneously interacting with ribosomal protein S10 in the ribosome 30S subunit[32-34]. When present, the coupling factor NusA forms a second bridge between RNAP and the ribosome; this second bridge supplements, but cannot substitute for, the bridge formed by NusG or RfaH (Fig. 1)[33-34].

Structures of NusG- and RfaH-coupled TTC-B have been obtained using nucleic-acid scaffolds for mRNA spacers between RNAP and ribosome that were 7, 8, 9, or 10 codons in length (21, 24, 27, or 30 nt in length) (Fig. 1)[32-34]. Structures of TTC-B having mRNA spacers 7, 8, 9, or 10 codons in length are superimposable[32-34], with the differences in mRNA spacer length being accommodated by different extents of compaction and disorder of mRNA in the RNAP-exit channel (Fig. 1)[32-34]. Based on the volume of the RNAP RNA-exit channel, the RNAP-exit channel is predicted to be able to accommodate a

maximum of 5 codons (15 nt) of compacted and disordered mRNA [33]; therefore, it is expected that TTC-B is compatible with, and can be formed, only for mRNA spacers of lengths ranging from 7 codons (21 nt) to 7 + 5 = 12 codons (36 nt)[33].

Qureshi and Duss[35] recently reported single-molecule fluorescence-resonance energy-transfer studies of *E. coli* transcription-translation coupling. Their results confirm the existence of functional and physical coupling between RNAP and ribosome, confirm the role of coupling factors NusG and NusA in enhancing coupling, and indicate, surprisingly, that coupling can occur not only over the range of RNAP-ribosome spacings that can be accmomodated in TTC-B, but also over much greater RNAP-ribosome spacings. Based on their findings, Qureshi and Duss conclude that there exists a structural class of TTCs that can accommodate very long mRNA spacers between RNAP and ribosome, accommodating these spacers by looping out of the mRNA spacer between RNAP and ribosome. Qureshi and Duss further conclude that the long-range coupling, although it clearly occurs, is less stable than short-range coupling. The lower stability is reflected in a smaller number of complexes observed with long-range coupling than with short-range coupling.

Here, in order to define the structural basis of transcription-translation coupling with long mRNA spacers between RNAP and ribosome, and to test the proposal of looping out of long mRNA spacers between RNAP and ribosome, we determined cryo-EM structures of *E. coli* NusG- and RfaH-coupled TTCs with mRNA spacers longer than those that can be accomnodated within TTC-B.

Structure determination

We assembled TTCs using synthetic nucleic-acid scaffolds analogous to those used previously to determine structures of NusG- and RfaH-coupled TTCs (Figs. 1, 2b, 3b)[32-34]. The scaffolds consist of three parts: (i) DNA and mRNA determinants that direct formation of a transcription elongation complex (TEC) upon addition of RNAP; (ii) an mRNA AUG codon that directs formation of a translation complex having the AUG codon in the ribosome active-center product site (P-site) upon addition of a ribosome and $tRNA^{fMet}$; and (iii) an mRNA spacer having, in intial studies, a length, *n*, of 12 or 13 codons, and in subsequent studies a length, *n*, of 17 or 20 codons (Figs. 2b, 3b). For determination of structures of

RfaH-coupled TTCs, the nucleic-acid scaffolds also contained an *ops* site with consensus sequence and positioning relative to the unwound transcription bubble of the TEC (Fig 1b, right subpanel). For each nucleic-acid scaffold, we equilibrated the scaffold with RNAP to form a TEC; we than added coupling factor NusG or RfaH, and optionally also coupling factor NusA, to form a NusG- or RfaH-containing TEC; and we than added ribosomes and $tRNA^{fMet}$ to form a NusG- or RfaH-containing TTC. For each resulting complex we than determined the structure using single-particle reconstruction cryo-EM (Extended Data Figs. 1-5; Extended Data Tables 1-2).

Structures of NusG- and RfaH-coupled TTCs containing long--12 or 13 codons--mRNA spacers between RNAP and ribosome

We first determined structures of NusG- and RfaH-containing TTCs using nucleic-acid scaffolds having mRNA spacers of length, *n*, of 12 and 13 codons, representing mRNA spacers that are at or above the expected maximum length mRNA spacer that can be accommodated in, and can enable formation of, TTC-B (Figs. 2-3; Extended Data Figs. 1-3; Extended Data Tables 1-2). Using these scaffolds, we obtained structures of NusG- or RfaH-coupled, NusA-co-coupled TTCs that define a new structural class of TTCs, different from TTC-B (Figs 2-3). In this new structural class of TTCs, the position of RNAP relative to the ribosome differs from that in a NusG-coupled TTC-B subclass B1 and in RfaH-coupled TTC-B by a rotation of ~60º and a translation of ~70Å (Figs. 2d, 3d; Extended Data Figs. 1f, 2f, 3f) and differs from the orientation in NusG-coupled TTC-B subclasses B2 and B3 by a rotation of ~45º and translation of ~63Å and a rotation of ~ 30º and translation of ~47Å, respectively (Extended Data Fig. 1f). In this new structural class of TTCs, in contrast to in previously defined structural class TTC-B, there is no, or almost no, interaction between RNAP and the ribosome (Figs. 2e-h, 3e-h). The new structural class also differs from TTC-B in the path of mRNA from RNAP to ribosome, having a ~70Å gap between mRNA in the RNAP RNA-exit channel and mRNA interacting with the ribosome, reflecting the ~70Å translation of RNAP relative to the ribosome in TTC-LC relative to TTC-B (Figs. 2d-h, 3d-h). Coupling occurs solely, or nearly solely, through the coupling factor NusG or RfaH and the second coupling factor NusA (Figs. 2e-f, 3e-f). We refer to this new structural class as "TTC-LC", where "LC" refers both to

long-range coupling and loose coupling, reflecting the association of this structural class with long mRNA spacers between ribosome and RNAP, and the absence or near-absence of direct interaction between RNAP and ribosome.

For NusG-coupled, NusA-co-coupled TTCs containing an mRNA spacer length of 12 codons, we obtained both TTC-B and TTC-LC (Figs. 2-3; Extended Data Fig. 1; Extended Data Table 1). For NusG-coupled, NusA-co-coupled TTCs containing an mRNA spacer of 13 codons, and for RfaH-coupled, NusA-co-coupled TTCs containing mRNA spacers of length of 12 or 13 codons, we obtained only TTC-LC (Figs. 2-3; Extended Data Figs. 2-3; Extended Data Tables 1-2). Based on our previous results analyzing structures of TTCs with shorter mRNA spacers and on these new results with 12 or 13 codon mRNA spacers, we infer that, as anticipated, TTC-B only can accommodate, and be formed with, mRNA spacers up to 11-12 codons in length, and we infer that the new structural class, TTC-LC, is formed for mRNA spacers ≥12 codons in length. Structures of TTC-LC for mRNA spacers of 12 codons and mRNA spacers of 13 codons are superimposable (Figs 2c, 3c). The difference sin mRNA spacer length are accommodated by different extents of compaction and disorder of mRNA inside the RNAP RNA-exit channel and in mRNA in the "gap" between the RNAP RNA exit-channel and mRNA associated with the ribosome (Figs. 2e-f, 3e-f). Structures of the NusG-coupled, NusA-co-coupled TTC-LC and RfaH-coupled, NusA-co-coupled TTC-LC are superimposable (Figs. 2a, 3a).

Reflecting the difference in orientatons of RNAP relative to the ribosome in TTC-B and TTC-LC, there are major differences in the interface between TEC and the ribosome in TTC-B and TTC-LC (Figs. 2e-h, 3e-h). In contrast to TTC-B, where the RNAP β' zinc binding domain (β' ZBD) makes direct protein-protein interaction with ribosomal protein S3 in the ribosome 30S subunit (314 $Å^2$ buried surface area; Figs. 2g-h., 3g-h)[32-34], in TTC-LC, RNAP makes no interactions with ribosomal protein S3 and makes no or almost no interactions with any other part of the ribosome, making at most contacts through 1-3 amino acids of the RNAP β' zinc binding domain (ZBD) with ribosomal protein S10 (0-56 $Å^2$; buried surface area; Figs. 2e-h, 3e-h).

In both TTC-B and TTC-LC, coupling factor NusG or RfaH bridges RNAP and the ribosome, with NusG-N or RfaH-N interacting with RNAP and NusG-C or RfaH-C interacting with ribosomal protein S10 in the ribosome 30S subunit (Figs. 2a, 2e-f, 3a, 3e-f). However, reflecting the difference in orientatons of RNAP relative to the ribosome in TTC-B and TTC-LC, there is a major difference in the orientation of of NusG-N or RfaH-N relative to NusG-C or RfaH-C in TTC-B and TTC-LC (Figs. 2e-h, 3e-h). The difference in orientation is accommodated by a change in the conformation of the NusG or RfaH interdomain linker (Figs. 2e-h, 3e-h).

In both TTC-B and TTC-LC, coupling factor NusA makes a second bridge between RNAP and the ribosome (Figs. 1a-b, 2a, 2e-h, 3a, 3e-h). However, reflecting the difference in orientatons of RNAP relative to the ribosome in TTC-B and TTC-LC, there are major differences in the bridging by NusA in TTC-B and TTC-LC (Figs. 2e-h, 3e-h). In TTC-B, the bridging by NusA involves extensive protein-protein interaction between NusA and ribosomal proteins S2 and S5 in the ribosome 30S subunit (Figs. 2g-h, 3g-h)[33-34]; in contrast, in TTC-LC, the bridging involves no protein-protein interactions between NusA and ribosomal proteins and is only indirect, involving only interactions between NusA and one face of the mRNA segment that, through its opposite face, interacts with ribosomal protein S3 in the ribosome 30S subunit (Figs. 2e-f, 3e-f).

In contrast to TTC-B, where mRNA proceeds directly from the RNAP RNA-exit channel to the RNA-helicase region[36] of ribosomal protein S3 in the ribosome 30S subunit[32-34] (Figs. 2g-h, 3g-h), in TTC-LC, there is a ~70 Å gap between mRNA in the RNAP RNA-exit channel and mRNA interacting with the RNA-helicase region[36] of ribosomal protein S3 in the ribosome 30S subunit (Figs. 2e-f, 3e-f, 4a-b). In our structures of TTC-LC, this mRNA segment is disordered (Figs. 2e-f, 3e-f, 4a-b); nevertheless, molecular modeling indicates that this mRNA segment makes no interactions with RNAP, coupling factors, or the ribosome, and indicate that this mRNA segment occupies a ~45 Å wide, ~70 Å long, solvent channel providing accessibility to bulk solvent outside TTC-LC (Fig 4a-b).

We also have sought cryo-EM structures of NusG- and RfaH-coupled complexes containing mRNA spacers of 12 and 13 codons in the absence of the co-coupling factor NusA (Extended Data Figs. 4-5).

Maps obtained in the absence of NusA show unequivocal density for RNAP interacting with the ribosome, and the density occupies a position that is superimposable on the position of density for TTC-LC obtained in the presence of NusA (Extended Data Figs. 4e-f, 5e-f). In the absence of NusA, map quality for RNAP is insufficient to define a unique fit and atomic model for RNAP interacting with the ribosome (Extended Data Figs. 4e, 5e), but density is decidedly clearer and decidedly more focused than density for "uncoupled TTCs" formed in the absence of NusG or RfaH (see ref. 31). We suggest that NusG- and RfaH-coupled TTC-LC can be formed both in the presence and in the absence of co-coupling factor NusA, but that the conformational heterogeneity and flexibility of the coupling is higher in the absence of NusA than in the presence.

Structures of NusG-coupled TTCs containing very long--17 or 20 codons--mRNA spacers between RNAP and ribosome

In both NusG- and RfaH-coupled TTC-LC, the mRNA segment in the ~70 Å gap between the mRNA in the RNAP RNA-exit channel and mRNA interacting with the RNA-helicase region of ribosomal protein S3 in the ribosome appears not to be engaged in protein-RNA interactions and occupies a ~45 Å wide, ~70 Å long solvent channel providing accessibility to bulk solvent the outside TTC-LC (Figs. 2e-f, 3e-f, 4-b). Thes observations suggest there likely are no constraints on the length or path of this mRNA segment and, thus, that lomger mRNA spacers potentially can be accommodated through mRNA looping in this mRNA segment.

To test this hypothesis, in further studies, we determined structures of NusG-containing, NusA-containing TTCs having very lomg--17 codon and 20 codon (54 nt and 60 nt)--mRNA spacers (Fig. 2b). A 17 codon mRNA spacer exceeds the maximum-length mRNA spacer that can be accommodated solely through compaction and disorder in the RNAP RNA-exit channel of TTC-LC without mRNA looping, and a 20 codon mRNA spacer substantially exceeds the maximum-length spacer that could be accommodated solely through compaction and disorder in the RNAP RNA-exit channel without mRNA looping.

We obtained structures of NusG-coupled, NusA-co-coupled TTC-LC having 17 codon and 20 codon mRNA mRNA spacers (Figs. 2c, 4a-b; Extended Data Fig. 2d-e). The structures were superimposable on

structures of NusG-coupled, NusA-co-coupled TTC-LC having 12 codon and 13 codon mRNA spacerss (Extended Data Fig. 2f). As in the structures having 12 codon and 13 codon mRNA spacers,, mRNA in the RNAP RNA-exit channel and in the ~70 Å gap between mRNA in the RNAP RNA-exit channel and mRNA interacting with the ribosome was disordered (Fig. 4a-b). Nevertheless, because a 17 codon mRNA spacer exceeds the maximum length of mRNA spacer that can be accommodated through compaction and disorder of mRNA in the RNAP RNA-exit channel, and because a 20 codon mRNA spacer substantially exceeds the maximum length of mRNA spacer that can be accommodated through compaction and disorder of mRNA in the RNAP RNA-exit channel, we conclude that mRNA in the ~70 Å gap in the structures with 17 codon and 20 codon mRNA spacers must be accommodated through mRNA looping (Fig. 4a.b).

Discussion

Our results define a new structural class of NusG- and RfaH-coupled TTCs. This new class accommodates mRNA spacers between RNAP and the ribosome that are longer than those that can be accommodated by the previously defined structural class TTC-B. In this new structural class, there is no or almost no direct interaction between RNAP and the ribosome. Coupling is mediated by bridging of RNAP and the ribosome through the coupling factor NusG or RfaH and by supplementary indirect bridging of RNAP and the ribosome through the coupling factor NusA. In this new structural class, there is a ~70 Å gap between mRNA in the RNAP RNA-exit channel and mRNA interacting with the ribosome 30S subunit. mRNA in the ~70 Å gap appears to make no protein-RNA interactions and to be accessible to the exterior of TTC-LC through a ~45 Å wide, ~70 Å long, solvent channel. In this new structural class, mRNA in the ~70 Å gap can accommodate very long, potentially unlimited-lengh, mRNA spacers through RNA looping. We refer to this new class as "TTC-LC." where "LC" denotes both long-range coupling, reflecting the fact that this class is associated with long mRNA spacers, and loose coupling, reflecting the absence or near absence of direct RNAP-ribosome interaction.

This new structural state, TTC-LC, explains, and accounts for, the single-molecule fluorescence-resonance energy-transfer observations of Qureshi and Duss[35]. Specifically, this TTC-LC enables long-range coupling with very long mRNA spacers between RNAP and the ribosome, involves coupling through NusG or RfaH and NusA, and involves, due to the absence or near absence of RNAP-ribosome interaction, a lower stability of coupling[35].

We propose that TTC-LC is a functional coupling complex and serves as a functional intermediate in forming and disassembling TTC-B (Fig. 4c). We hypothesize that TTC-LC mediates transcription-coupled translation initiation when the mRNA spacer between RNAP and the translation start codon is longer than the maximum spacer length compatible with formation of TTC-B--which occurs frequently, in view of the relatively late loading of NusG and RfaH onto RNAP[9,37-38]--and then mediates pre-TTC-B transcription-translation coupling, until the ribosome "catches up" to RNAP and forms TTC-B (Fig, 4, left and center). We also hypothesize that TTC-LC mediates "post-TTC-B" transcription-translation coupling when the ribosome stops moving but RNAP continues moving, resulting in an mRNA spacer length longer than the maximum spacer length compatible with TTC-B (Fig 4, right). The observation that NusG and RfaH often load onto RNAP at positions downstream of the translation start codon that would yield mRNA spacers between RNAP and the ribosome substantially longer than those that can be accommodated in TTC-B[9,37-38] has posed a challenge to the hypothesis that TTC-B functionally mediates transcription-translation coupling[9,12-13]. The discovery of this new structural class, TTC-LC, able to mediate transcription-translation coupling with substantially longer mRNA spacers, resolves this challenge.

The structural differences between TTC-B and TTC-LC predict functional differences between TTC-B and TTC-LC in terms of suppression of pausing and termination. Molecular modeling indicates that TTC-LC, unlike TTC-B, can accommodate a pause RNA hairpin[39-40] or a termination RNA hairpin[41] without steric clash and without interaction of the pause or termination hairpin with the RNA-helicase region of ribosomal protein S3, with the pause or termination hairpin being accommodated within the ~70Å gap region of TTC-LC (Extended Data Fig. 6a). We therefore infer that, unlike TTC-B, in which

the pause or termination hairpin would interact with the with the RNA-helicase region of ribosomal protein S3[32-34], TTC-LC will not suppress hairpin-dependent transcription pausing and hairpin-dependent transcription termination. Molecular modeling indicates that like TTC-B, TTC-LC is incompatible with formation of a transcription pre-termination complex containing the transcription termination factor Rho[24] (Extended Data Fig. 6b). We therefore infer that, like TTC-B, TTC-LC will suppress Rho-dependent transcription termination.

Key priorities for future work include demonstration that both TTC-B and TTC-LC are present in cells, by use of *in situ* structural biology through cryo-electron tomography[42], and assessment of the effects of TTC-LC on transcription pausing and transcription termination, by use of the single-molecule fluorescence resonance energy transfer assays of Qureshi and Duss[35].

Acknowledgments

We thank the Rutgers CryoEM and Nanoimaging Facility and the Stanford-SLAC Cryo-EM Center (supported by NIH grant GM129541), for microscope access. We thank Emre Firlar for technical assistance with cryo-EM data collection.

Funding

This work was supported by National Institutes of Health (NIH) grant GM041376 to R.H.E.

Author contributions

C.W., V.M., and R.H.E. designed experiments. V.M. and G.B. prepared proteins and nucleic acids. V.M, C.W., and J.T.K. performed cryo-EM data collection. V.M., C.W., and R.H.E. analyzed data. C.W.m V.W., and R.H.E. prepared figures. R.H.E. wrote the manuscript.

Competing interests

The authors declare no competing interests.

Data availability statement

Cryo-EM maps have been deposited in the Electron Microscopy Database (EMDB accession codes 43335, 43387, 43388, 43389, 43390, and 43391, and atomic coordinates have been deposited in the Protein Database (PDB accession codes 8VL1, 8VOO, 8VOP, 8VOQ, 8VOR, and 8VOS). Unique biological materials will be made available to qualified investigators on request.

References

1. Byrne, R., Levin, J.G., Bladen, H.A. & Nirenberg, M.W. (1964) The in vitro formation of a DNA-ribosome complex. *Proc. Natl. Acad. Sci. USA* **52**, 140-148.

2. Miller, O., Hamkalo, B. & Thomas, C. (1970) Visualization of bacterial genes in action. *Science* **169**, 392-395.

3. Proshkin, S., Rahmouni, A., Mironov, A. & Nudler, E. (2010) Cooperation between translating ribosomes and RNA polymerase in transcription elongation. *Science. 2010 Apr 23;* **328**, 504-508.

4. Burmann, B., Schweimer, K., Luo, X., Wahl, M., Stitt, B., Gottesman, M. & Rösch, P. (2010) A NusE:NusG complex links transcription and translation. *Science* **328**, 501-504.

5. Burmann, B., Knauer, S., Sevostyanova, A., Schweimer, K., Mooney, R., Landick, R., Artsimovitch, I. & Rosch, P. (2012) An α helix to β barrel domain switch transforms the transcription factor RfaH into a translation factor. *Cell* **150**, 291-303.

6. McGary, K. & Nudler, E. (2013) RNA polymerase and the ribosome: the close relationship. *Curr. Opin. Microbiol.* **16**, 112-117.

7. Artsimovitch, I. (2018) Rebuilding the bridge between transcription and translation. *Mol. Microbiol.* **108**, 467-472.

8. Saxena, S., Myka, K., Washburn, R., Costantino, N., Court, L. & Gottesman, E. (2018) *Escherichia coli* transcription factor NusG binds to 70S ribosomes. *Mol. Microbiol.* **108**, 495-504.

9. Washburn, R., Zuber, P., Sun, M., Hashem, Y., Shen, B., Li, W., Harvey, S., Acosta Reyes, F., Gottesman, M., Knauer, S. & Frank, J. (2020) *Escherichia coli* NusG links the lead ribosome with the transcription elongation complex. *iScience* **23**, 101352.

10. Chatterjee, S., Chauvier, A., Dandpat, S., Artsimovitch, I. & Walter, N. (2021) A translational riboswitch coordinates nascent transcription-translation coupling. *Proc. Natl. Acad. Sci. USA* **118**, e2023426118.

11. Webster, M. & Weixlbaumer, A. (2021) Macromolecular assemblies supporting transcription-translation coupling. *Transcription* **12**, 103-125.

12. Irastortza-Olaziregi, M. & Amster-Choder, O. (2020) Coupled transcription-translation in prokaryotes. Front. Microbiol. 11, 624830.

13. Blaha, G. & Wade, J. (2022) Transcription-translation coupling in bacteria. *Annu. Rev. Genet.* **56**, 9.1-9.19.

14. Bailey, E., Gottesman, M. & Gonzalez, R., Jr. (2022) NusG-mediated coupling of transcription and translation enhances gene expression by suppressing RNA polymerase backtracking. *J. Mol. Biol.* **434**, 167330.

15. Stevenson-Jones, F., Woodgate, J., Castro-Roa, D. & Zenkin, N. (2020) Ribosome reactivates transcription by physically pushing RNA polymerase out of transcription arrest. *Proc. Natl. Acad. Sci. USA* **117**, 8462-8467.

16. Wee, L.M., Tong, A.B., Florez Ariza, A.J., Canari-Chumpitaz, C., Grob, P., Nogales, E. & Bustamante, C.J. (2023) A trailing ribosome speeds up RNA polymerase at the expense of transcript fidelity via force and allostery. *Cell* **186**, 1244-1262.

17. Landick, R., Carey, J. & Yanofsky, C. (1985) Translation activates the paused transcription complex and restores transcription of the *trp* operon leader region. *Proc Natl Acad Sci U S A* **82**, 4663-4667.

18. Roland, K., Liu, C. & Turnbough, C. (1988) Role of the ribosome in suppressing transcriptional termination at the pyrB1 attenuator of Escherichia coli. *Proc. Natl. Acad. Sci. USA* **85**, 7149-7153.

19. Peters, J., Vangeloff, A. & Landick, R. (2011) Bacterial transcription terminators. *J. Mol. Biol.* **412**, 793-813.

20. Ray-Soni, A., Bellecourt, M. & Landick, R. (2016) Mechanisms of bacterial transcription termination. *Annu. Rev. Biochem.* **85**, 319-347.

21. Mitra, P., Ghosh, G., Hafeezunnisa, M. & Sen, R. (2017) Rho protein: roles and mechanisms. *Annu. Rev. Microbiol.* **71**, 687-709.

22. Roberts, J. (2019) Mechanisms of bacterial transcription termination. *J. Mol. Biol.* **431**, 4030-4039.

23. Sunday, N., Svetlov, D. & Artsimovitch, I. (2021) Rho termination factor: one ring to bind them all. In *RNA Polymerases as Molecular Motors, Second Edition*, eds. Landick, R., Wang, J. & Strick, T. (Cambridge, United Kingdom, RSC Publishing), pp. 100-131.

24. Molodtsov, V., Wang, C., Firlar, E., Kaelber, J. & Ebright, R.H. (2023) Structural basis of Rho-dependent transcription termination. *Nature* **614**, 367-374.

25. Burmann, B.M. & Rosch, P. (2011) The role of *E. coli* Nus-factors in transcription regulation and transcription: translation coupling. *Transcription* **2**, 130-134.

26. Werner, F. (2012) A nexus for gene expression-molecular mechanisms of Spt5 and NusG in the three domains of life. *J. Mol. Biol.* **417**, 13-27.

27. Tomar, S. & Artsimovitch, I. (2013) NusG-Spt5 proteins-universal tools for transcription modification and communication. *Chem. Rev.* **113**, 8604-8619.

28. Artsimovitch, I. & Knauer, S.H. (2019) Ancient transcription factors. *mBio* **10**:e01547-18.

29. Wang, B. & Artsimovitch, I. (2021) NusG, an ancient yet rapidly evolving transcription factor. *Front. Microbiol.* **11**, 619618.

30. Strauss, M., Vitiello, C., Schweimer, K., Gottesman, M., Rosch, P. & Knauer, S. (2016) Transcription is regulated by NusA:NusG interaction. *Nucl. Acids Res.* **44**, 5971-5982.

31. Kohler, R., Mooney, A., Mills, J., Landick, R. & Cramer, P. (2017) Architecture of a transcribing-translating expressome. *Science* **356**, 194-197.

32. Webster, M., Takacs, M., Zhu, C., Vidmar, V., Eduljee, A., Abdelkareem, M. & Weixlbaumer, A. (2020) Structural basis of transcription-translation coupling and collision in bacteria. *Science* **369**, 1355-1359.

33. Wang, C., Molodtsov, V., Firlar, E., Kaelber, J., Blaha, G., Su, M. & Ebright, R.H. (2020) Structural basis of transcription-translation coupling. *Science* **369**, 1359-1365.

34. Molodtsov, V., Wang, C., Zhang, J., Kaelber, J., Blaha, G,, and Ebright, R.H. (2024) Structural basis of RfaH-dependent transcription-translation coupling. *Nature Structl. Mol. Biol.* (in press; https://www.biorxiv.org/content/10.1101/2023.11.05.565726v1).

35. Qureshi, N.S. & Duss, O. (2023) Tracking transcription-translation coupling in real-time. https://www.biorxiv.org/content/10.1101/2023.12.07.570708v1.

36. Takyar, S., Hickerson, R., and Noller, H. (2005) mRNA helicase activity of the ribosome. *Cell* **120**, 49-58.

37. Mooney, R., Davis, S., Peters, J., Rowland, J., Ansari, A. & Landick, R. (2009) Regulator trafficking on bacterial transcription units *in vivo*. *Mol. Cell* **33**, 97-108.

38. Belogurov, G., Mooney, R., Svetlov, V., Landick, R. & Artsimovitch, I. (2009) Functional specialization of transcription elongation factors. *EMBO J.* **28**, 112-122.

39. Kang, Y., Mishanina, V., Bellecourt, J., Mooney, A., Darst, S., & Landick, R. (2018) RNA polymerase accommodates a pause RNA hairpin by global conformational rearrangements that prolong pausing, *Mol. Cell* **69**, 802-815.

40. Guo, X., Myasnikov, G., Chen, J., Crucifix, C., Papai, G., Takacs, M., Schultz, P. & Weixlbaumer, A. (2018) Structural basis for NusA stabilized transcriptional pausing, *Mol. Cell* **69**, 816-827.

41. You, L, Omollo, E., Yu, C., Mooney, R., Shi, J., Shen, L., Wu, X., Wen, A., He, D., Zeng, Y., Feng, Y., Landick, R. &Zhang Y. Structural basis for intrinsic transcription termination. (2023) *Nature* **613**, 783-789.

42. Tegunov, D., Xue, L., Dienemann, C., Cramer, P. & Mahamid, J. (2021) Multi-particle cryo-EM refinement with M visualizes ribosome-antibiotic complex at 3.5 A in cells. *Nature Meths*. **18**, 186-193.

Figure legends

Fig. 1. Structures of NusG-, NusA-coupled TTC-B and RfaH-, NusA-coupled TTC-B

(a) NusA-NusG-TTC-B (PDB 6X6T)[33]. Left: structure. Top right: nucleic-acid scaffold used for structure determination. Bottom right: accommodation of different mRNA spacer lengths in NusA-NusG-TTC-B.

(b) NusA-RfaH-TTC-B (PDB 8UQP).[34] Left: structure. Top right: nucleic-acid scaffold used for structure determination (*ops* site in grey and underlined). Bottom right: accommodation of different mRNA spacer lengths in NusA-RfaH-TTC-B.

Left panels show EM density (grey surface) and fit (ribbons) for TEC, NusG or RfaH, and NusA (at top), and for ribosome 30S and 50S subunits and P-site and E-site tRNAs (at bottom). RNAP β', β, α^1, α^2, and ω subunits are in pink, cyan, light green, green, and grey; 30S subunt, 50S subunit, P-site tRNA, and E-site tRNA are in yellow, grey, green, and orange; DNA non-template strand, DNA template strand, and mRNA are in black, blue, and brick-red; NusG or RfaH, NusA, and ribosomal protein S10 are in red, light blue, and magenta; ribosome L7/L12 stalk is omitted for clarity in this and subsequent images.

Top right subpanels show nucleic-acid scaffolds used for structure determination, Each scaffold comprises non-template-strand oligodeoxyribonucleotide (black), template-strand oligodeoxyribonucleotide (blue), and mRNA oligoribonucleotide (brick red). Dashed box labeled "TEC," portion of nucleic-acid scaffold that forms TEC upon addition of RNAP (10 nt non-template- and template-strand ssDNA segments forming "transcription bubble," 9 nt of mRNA engaged with templat-strand DNA as RNA-DNA "hybrid," and 5 nt of mRNA, on diagonal, in RNAP RNA-exit channel); red box labeled "ribosome P-site," mRNA AUG codon intended to occupy ribosome active-center P-site upon addition of ribosome and $tRNA^{fMet}$.

Bottom right subpanels show accommodation of different mRNA spacer lengths inside complex. EM density, blue mesh; mRNA, brick red (disordered mRNA nucleotides indicated by dashed ovals); template-strand DNA in RNA-DNA hybrid, blue; RNAP active-center catalytic Mg^{2+}, purple sphere; ribosomal protein S3 in ribosome 30S subunit, orange; tRNA in ribosome P-site, green. Pairs of diagonal black lines indicate edges of RNAP and ribosome.

Fig. 2. Structure of NusG-, NusA-coupled TTC-LC

(a) Structure of NusG-NusA-TTC-LC (n = 17, Extended Data Table 1). Two orthogonal views. Colors as in Fig. 1.

(b) Nucleic-acid scaffold used for structure determination. Colors as in Fig. 1.

(c) EM density maps for structures of NusG-NusA-TTC-LC obtained using nucleic-acid scaffolds with n = 12, 13, 17, and 20 (superimposition at left; individual EM maps and color scheme at right). View orientation as in (a).

(d) Superimposition of NusA-NusG-TTC-LC (TEC in yellow and ribosome in grey) on NusA-NusG-TTC-B[33] (subclass B1; TEC in pink and ribosome in grey).

(e) RNAP-ribosome interface in NusA-NusG-TTC-LC (n = 17; identical interfaces for n = 12, 13, and 20). RNAP β' zinc binding domain (ZBD), pink with Zn^{2+} ion as black sphere; NusG, red; NusA, slate blue; ribosomal protein S3, orange; ribosomal protein S10, magenta; DNA template strand, blue; mRNA, brick red; disordered mRNA segment, black dashed oval; portions of RNAP β', β, and ribosome 30S not involved in the interactions are shaded pink, cyan, and yellow, respectively. In TTC-LC, NusG directly bridges RNAP and ribosome, with NusG-N interacting with RNAP, and NusG-C interacting with ribosomal protein S10. and NusA indirectly bridges RNAP and the mRNA segment interacting with ribosomal protein S3.

(f) As (e), showing cryo-EM density as blue mesh.

(g) RNAP-ribosome interface in NusA-NusG-TTC-B (n = 12)[33]. View orientation as in (e-f). In TTC-B, RNAP ZBD interacts with ribosomal protein S3; NusG directly bridges RNAP and ribosome, interacting with RNAP and ribosomal protein S2 (forest green) and S5 (brown); and NusA directly bridges RNAP and ribosome, interacting with RNAP and ribosomal protein S3.

(h) As (f), but for NusA-NusG-TTC-B (n = 12)[33].

Fig. 3. Structure of RfaH-, NusA-coupled TTC-LC

(a) Structure of RfaH-NusA-TTC-LC (n = 13, Extended Data Table 2). Views and colors as in Figs. 1 and 2a.

(b) Nucleic-acid scaffold used for structure determination. Colors as in Figs. 1 and 2b

(c) EM density maps for structures of RfaH-NusA-TTC-LC obtained using nucleic-acid scaffolds with n = 12 and 13 (superimposition at left; individual EM maps and color scheme at right). View orientation as in (a).

(d) Superimposition of RfaH-NusA-TTC-LC (TEC in yellow and ribosome in grey) on RfaH-NusA-TTC-B[34] (TEC in pink and ribosome in grey).

(e) RNAP-ribosome interface in RfaH-NusA-TTC-LC (n = 13; identical interfaces for n = 12). RfaH, red. Other colors as in Fig. 2e. In TTC-LC, RfaH directly bridges RNAP and ribosome, with RfaH-N interacting with RNAP and RfaH-C interacting with ribosomal protein S10; and NusA indirectly bridges RNAP and rivbosome, interacting with the mRNA segment that interacts with ribosomal protein S3.

(f) As (e), showing cryo-EM density as blue mesh.

(g) RNAP-ribosome interface in RfaH-NusA-TTC-B (n = 8)[34]. View orientation as in (e-f). In TTC-B, RNAP ZBD interacts with ribosomal protein S3; RfaH directly bridges RNAP and ribosome, interacting with RNAP and ribosomal protein S2 (forest green) and S5 (brown); and NusA directly bridges RNAP and ribosome, interacting with RNAP and ribosomal protein S3.

(h) As (f), but for RfaH-NusA-TTC-B.

Fig. 4. Accommodation of long mRNA spacers in TTC-LC through mRNA looping

(a) Inferred paths of mRNA spacers in NusA-NusG-TTC-LC. An mRNA spacer of 12 codons is accommodated without RNA looping (first brick-red dashed line, reading from left to right). mRNA spacers of 13, 17, and 20 codons (second, third, and fourth brick-red dashed lines, reading from left to right) are accommodated by progressively increasing extents of RNA looping into ~45 Å wide, ~70 Å long, solvent channel providing access to bulk solvent on exterior of TTC-LC (white space at center-right). Image shows view orientation that places segment of mRNA spacer in gap between mRNA in the RNAP RNA-exit channel (undashed brick-red ribbon at top) and mRNA interacting with ribosomal protein S3 in ribosome 30S subunit (solid brick-red ribbon at bottom) in plane of the image. Ribosome 30S subunit, yellow; other colors as in Figs. 1, 2a, and 3a.

(b) as (a), but for NusA-RfaH-TTC-LC.

(c) Proposal: TTC-LC serves as functional intermediate in assembling and disassembling TTC-B. Proposal has three steps (left, center, and right subpanels). In step 1 (left subpanel), TTC-LC mediates transcription-coupled translation initiation when mRNA spacer between RNAP and translation start codon is longer than maximum-length spacer compatible with TTC-B ($n \geq 12$), and performs pre-TTC-B loose transcription-translation coupling. Subpanel shows schematic representation of TTC-LC, with looped out mRNA spacer as brick-red dashed line at center, and shows structure of TTC-LC at bottom. In step 2 (center subpanel), after ribosome "catches up" with RNAP, complex undergoes transition from TTC-LC to TTC-B, with no looping out of mRNA spacer, and mediates tight transcription-translation coupling for most transcription and translation. In step 3 (right subpanel), when ribosome stops moving and RNAP continues moving, resulting in increase in mRNA spacer length beyond maximum-length spacer compatible with TTC-B, the complex undergoes transition from TTC-B to TTC-LC, with looped out mRNA spacer (brick-red dashed line), and performs post-TTC-B loose transcription-translation coupling as TTC-LC.

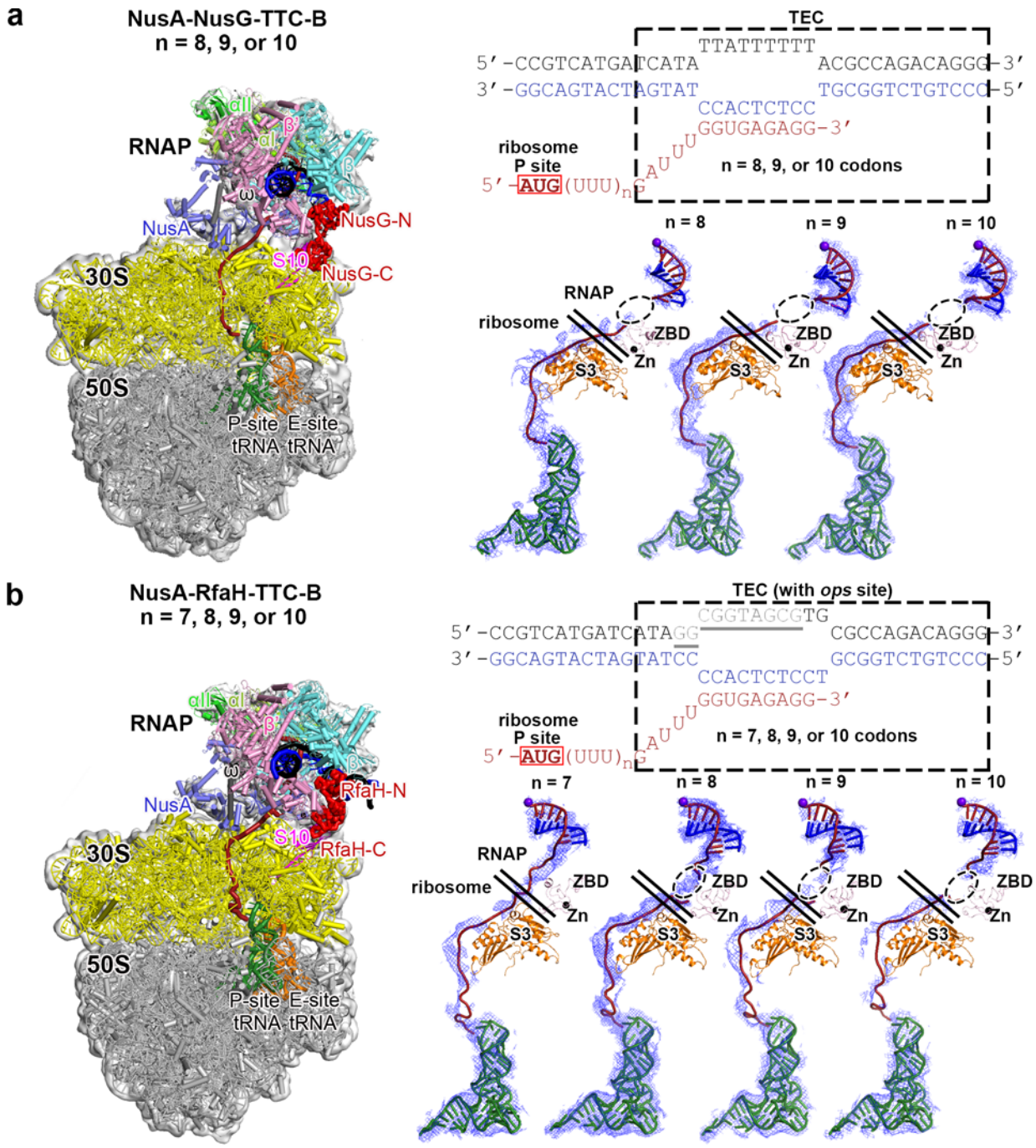
a
NusA-NusG-TTC-B
n = 8, 9, or 10
RNAP
αII
αI
β'
β
ω
NusA
NusG-N
S10
NusG-C
30S
50S
P-site tRNA
E-site tRNA
TEC
TTATTTTTT
5'-CCGTCATGATCATA
ACGCCAGACAGGG-3'
3'-GGCAGTACTAGTAT
TGCGGTCTGTCCC-5'
CCACTCTCC
GGUGAGAGG-3'
ribosome P site
5'-AUG(UUU)nGAUUU
n = 8, 9, or 10 codons
n = 8
n = 9
n = 10
RNAP
ribosome
ZBD
Zn
S3
b
NusA-RfaH-TTC-B
n = 7, 8, 9, or 10
RfaH-N
RfaH-C
TEC (with ops site)
CGGTAGCGTG
5'-CCGTCATGATCATAGG
CGCCAGACAGGG-3'
3'-GGCAGTACTAGTATCC
GCGGTCTGTCCC-5'
CCACTCTCCT
GGUGAGAGG-3'
n = 7, 8, 9, or 10 codons
n = 7
n = 8
n = 9
n = 10

Figure 1

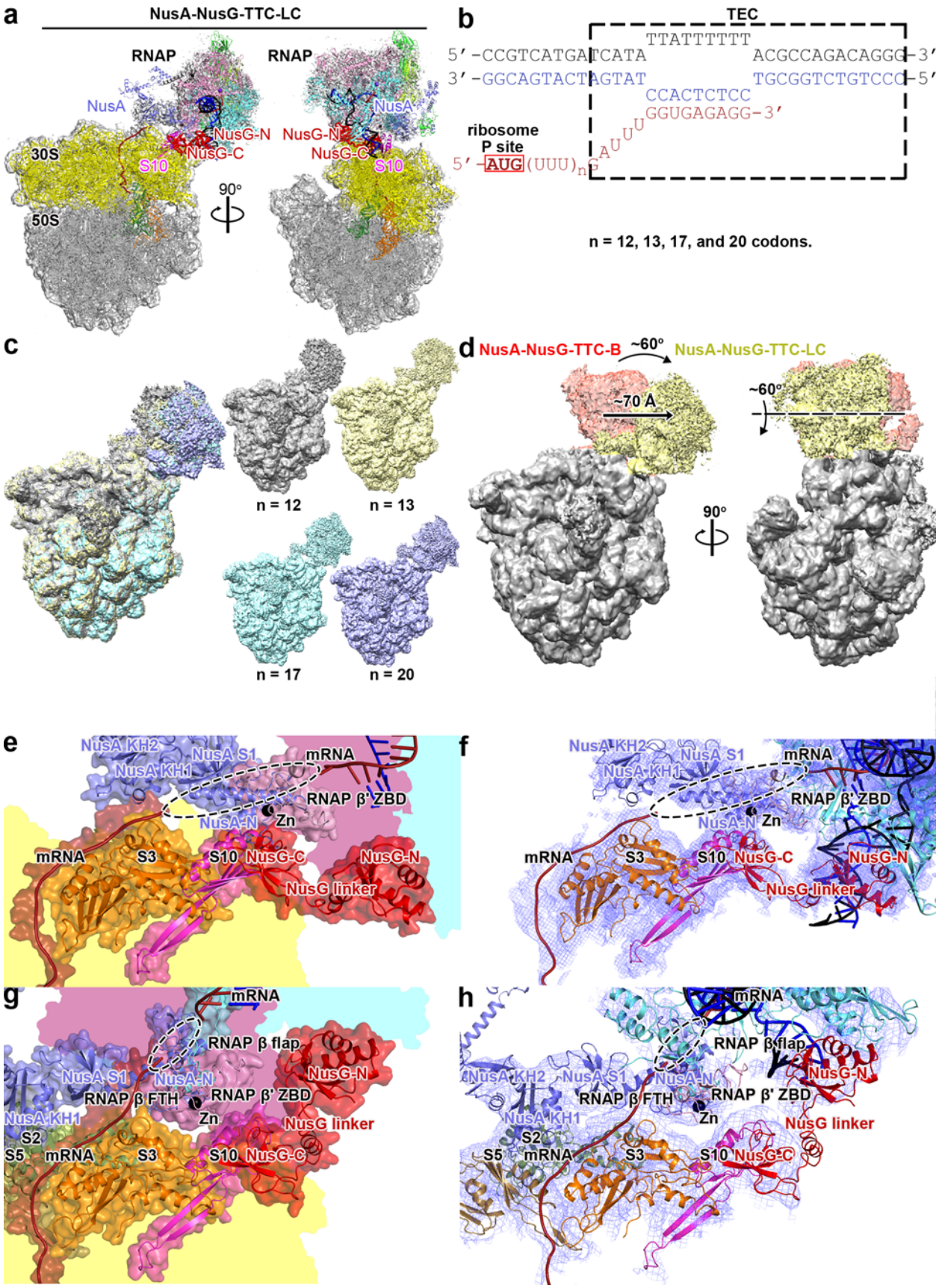
a
NusA-NusG-TTC-LC
RNAP
RNAP
NusA
NusA
NusG-N
NusG-N
NusG-C
NusG-C
30S
S10
S10
90°
50S
b
TEC
TTATTTTTT
5′-CCGTCATGATCATA
ACGCCAGACAGGG-3′
3′-GGCAGTACTAGTAT
TGCGGTCTGTCCC-5′
CCACTCTCC
GGUGAGAGG-3′
ribosome
P site
5′-AUG(UUU)nG
n = 12, 13, 17, and 20 codons.
c
n = 12
n = 13
n = 17
n = 20
d
NusA-NusG-TTC-B
~60°
NusA-NusG-TTC-LC
~70 Å
~60°
90°
e
NusA KH2
NusA S1
mRNA
NusA KH1
RNAP β' ZBD
NusA-N
Zn
mRNA
S3
S10
NusG-C
NusG-N
NusG linker
f
NusA KH2
NusA S1
mRNA
NusA KH1
RNAP β' ZBD
NusA-N
Zn
mRNA
S3
S10
NusG-C
NusG-N
NusG linker
g
mRNA
RNAP β flap
NusA S1
NusA-N
NusG-N
RNAP β FTH
RNAP β' ZBD
NusA KH1
Zn
NusG linker
S2
S5
mRNA
S3
S10
NusG-C
h
mRNA
RNAP β flap
NusA KH2
NusA S1
NusA-N
NusG-N
RNAP β FTH
RNAP β' ZBD
NusA KH1
Zn
NusG linker
S2
S5
mRNA
S3
S10
NusG-C

Figure 2

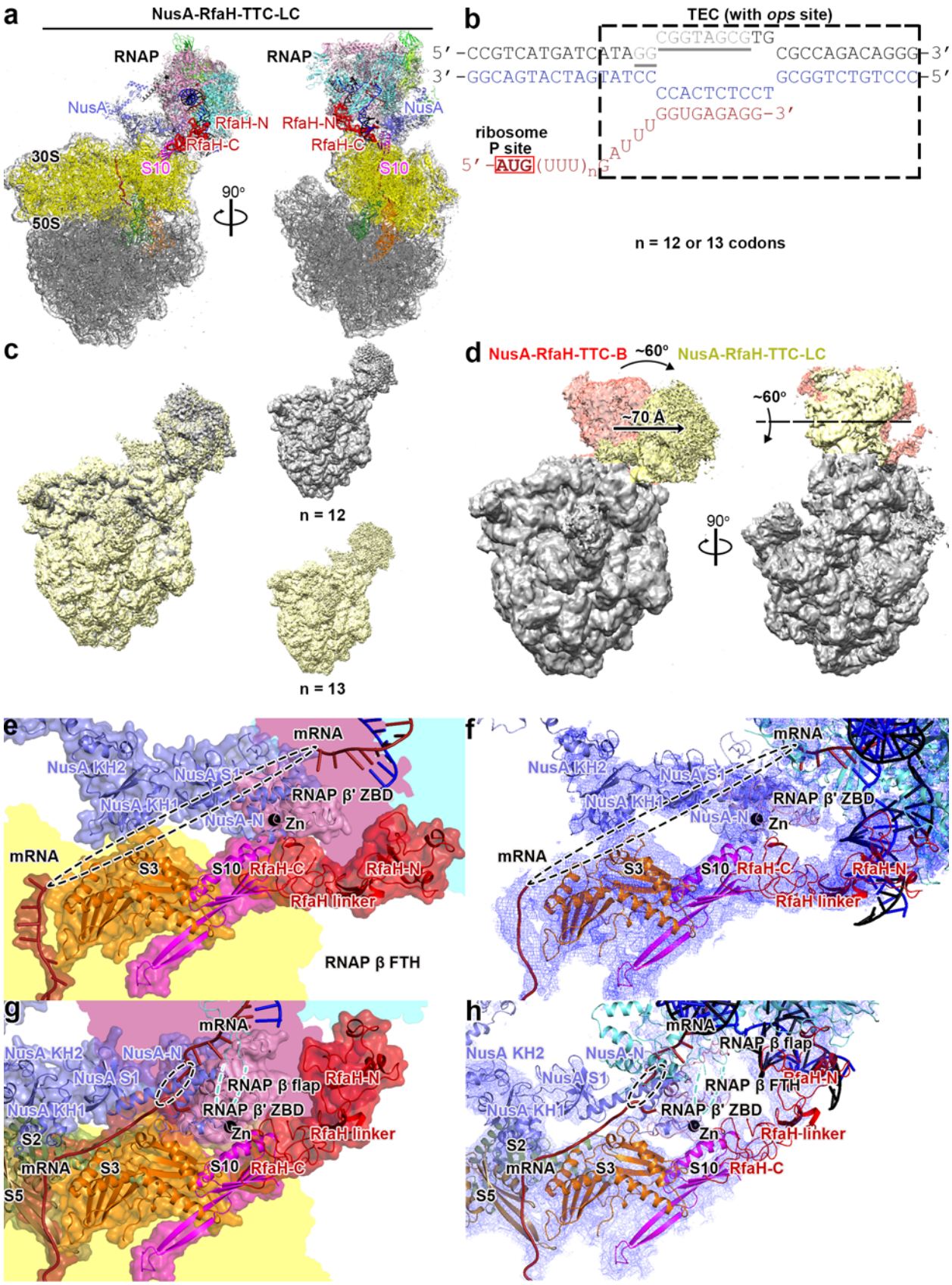
a
NusA-RfaH-TTC-LC
RNAP
RNAP
NusA
NusA
RfaH-N
RfaH-N
RfaH-C
RfaH-C
30S
S10
S10
90°
50S
b
TEC (with ops site)
CGGTAGCGTG
5′-CCGTCATGATCATAGG
CGCCAGACAGGG-3′
3′-GGCAGTACTAGTATCC
GCGGTCTGTCCC-5′
CCACTCTCCT
GGUGAGAGG-3′
ribosome
P site
5′-AUG(UUU)nG
n = 12 or 13 codons
c
n = 12
n = 13
d
NusA-RfaH-TTC-B
~60°
NusA-RfaH-TTC-LC
~70 Å
~60°
90°
e
mRNA
NusA KH2
NusA S1
NusA KH1
RNAP β' ZBD
NusA-N
Zn
mRNA
S3
S10
RfaH-C
RfaH-N
RfaH linker
RNAP β FTH
f
mRNA
NusA KH2
NusA S1
NusA KH1
RNAP β' ZBD
NusA-N
Zn
mRNA
S3
S10
RfaH-C
RfaH-N
RfaH linker
g
mRNA
NusA KH2
NusA-N
NusA S1
RNAP β flap
RfaH-N
NusA KH1
RNAP β' ZBD
Zn
RfaH linker
S2
mRNA
S3
S10
RfaH-C
S5
h
mRNA
RNAP β flap
NusA KH2
NusA-N
NusA S1
RNAP β FTH
RfaH-N
NusA KH1
RNAP β' ZBD
Zn
RfaH-linker
S2
mRNA
S3
S10
RfaH-C
S5

Figure 3

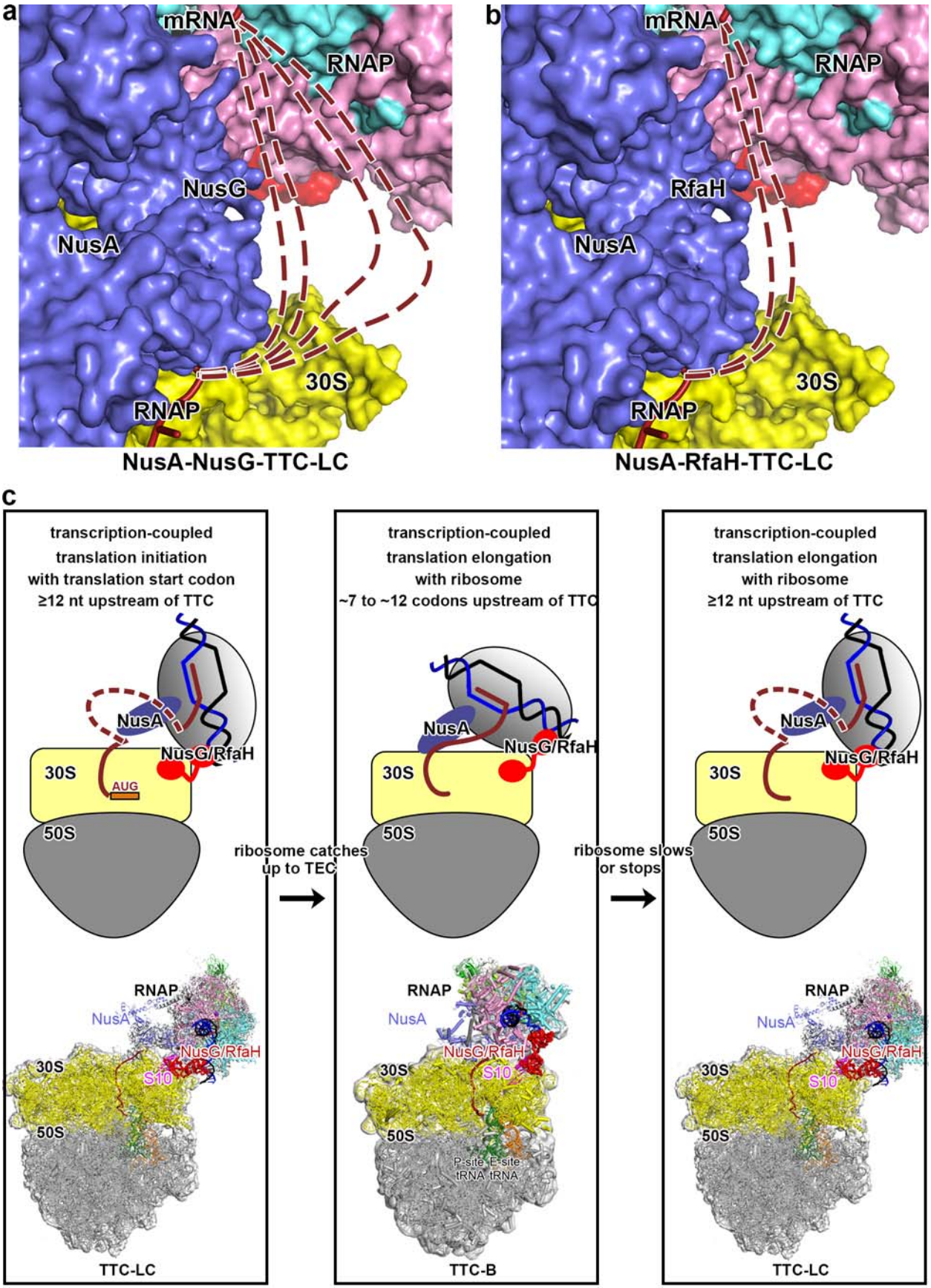
a
mRNA
RNAP
NusG
NusA
30S
RNAP
NusA-NusG-TTC-LC
b
mRNA
RNAP
RfaH
NusA
30S
RNAP
NusA-RfaH-TTC-LC
c
transcription-coupled
translation initiation
with translation start codon
≥12 nt upstream of TTC
NusA
NusG/RfaH
30S
AUG
50S
RNAP
NusA
NusG/RfaH
30S
S10
50S
TTC-LC
ribosome catches
up to TEC
transcription-coupled
translation elongation
with ribosome
~7 to ~12 codons upstream of TTC
NusA
NusG/RfaH
30S
50S
RNAP
NusA
NusG/RfaH
30S
S10
50S
P-site E-site
tRNA tRNA
TTC-B
ribosome slows
or stops
transcription-coupled
translation elongation
with ribosome
≥12 nt upstream of TTC
NusA
NusG/RfaH
30S
50S
RNAP
NusA
NusG/RfaH
30S
S10
50S
TTC-LC

Figure 4

Methods

E. coli RNAP core enzyme, NusA, NusG, RfaH, and 70S ribosomes

E. coli RNAP core enzyme, NusA, NusG, and 70S ribosomes were prepared as described[33]. *E. coli* RfaH^{E48A}, an RfaH derivative that contains a substitution in RfaH-N that disrupts interactions between RfaH-N and RfaH-C that stabilize an inactive conformational state of RfaH[5], was prepared as described[34].

E. coli tRNA^{fMet}

E. coli tRNA^{fMet} was purchased (MP Biomedical), dissolved to 100 µM in 5 mM Tris-HCl, pH 7.5, and stored in aliquots at -80°C.

Nucleic-acid scaffolds

Oligodeoxyribonucleotides and oligoribonucleotides (sequences in Figs. 2b and 3b) were purchased (Integrated DNA Technologies), PAGE-purified, dissolved in annealing buffer (5 mM Tris-HCl, pH 7.5) to 1 mM, and stored at -80°C in aliquots. Nucleic-acid scaffolds (sequences in Fig. 1b-c) were prepared as decribed[33-34], mixing 60 mM nontemplate-strand oligodeoxyribonucleotide, 60 mM template-strand oligodeoxyribonucleotide, and 60 mM oligoribonucleotide in 100 µl annealing buffer (5 mM Tris-HCl, pH 7.5), heating 10 min at 95ºC, and cooling slowly (3 h) to 22º, and nucleic-acid scaffolds were stored in aliquots at -80ºC.

Cryo-EM structure determination: sample preparation

TTCs were prepared as described[33-34], mixing 10 µl 20 µM RNAP core enzyme (in RNAP storage buffer: 10 mM Tris-HCl, pH 7.6, 100 mM NaCl, 0.1 mM EDTA, and 5 mM dithiothreitol), 0 or 30 ml 30 mM NusG or RfaH^{E48A} (in RNAP storage buffer), 0 or 16 ml 60 mM NusA (in RNAP storage buffer), 4 µl 60 µM nucleic-acid scaffold (in 5 mM Tris-HCl, pH 7.5), 10 ml 10x 70S ribosome storage buffer (20 mM Tris-HCl, pH 7.5, 30 mM KCl, 20 mM $Mg(OAc)_2$, and 4 mM 2-mercaptoethanol), and 26 ml (reactions without NusA) or 10 ml (reactions with NusA) water; incubating 10 min at 22ºC; adding 10 µl 100 µM

$tRNA^{fMet}$ (in 5 mM Tris-HCl, pH 7.5), 5 µl 40 µM 70S ribosome (in 70S ribosome storage buffer), and 5 ml water; and further incubating 10 min at 22ºC. The resulting TTCs were transferred to pre-chilled 0.5 ml Amicon Ultracel 30K concentrators (EMD Millipore), concentrated to 35 µl by centrifugation (15 min at 20,000xg at 4ºC), incubated 30 min on ice for 30 min, supplemented with 3.8 µl of ice-cold 80 mM CHAPSO, and immediately applied to grids.

EM grids were prepared as described[33-34], using a Vitrobot Mark IV autoplunger (FEI/ThermoFisher), with the environmental chamber at 22°C and 100% relative humidity. Samples (3 µl) were applied to 2/1 Quantifoil Cu 300 holey-carbon grids (Quantifoil); glow-discharged 60 s using a PELCO glow-discharge system (Ted Pella)]), grids were blotted with #595 filter paper (Ted Pella) for 7 s at 22°C, and grids were flash-frozen by plunging in a liquid ethane cooled with liquid N_2, and grids were stored in liquid N_2.

Cryo-EM structure determination: data collection and data reduction

Cryo-EM data for NusA-NusG-TTC-B (n = 12) and NusA-NusG-TTC-LC (n = 12), NusA-NusG-TTC-LC (n = 13), NusA-NusG-TTC-LC (n = 17), NusA-NusG-TTC-LC (n = 20), and NusA-RfaH-TTC-LC (n = 12) were collected at the Rutgers University Cryo-EM and Nanoimaging Core Facility, using a 200 kV Talos Arctica (FEI/ThermoFisher) electron microscope equipped with a GIF Quantum K2 direct electron detector (Gatan) (Extended Data Figs. 1-3). Data were collected automatically in counting mode, using EPU (FEI/ThermoFisher), a nominal magnification of 130,000x, a calibrated pixel size of 1.038 Å/pixel, and a dose rate of 4.8 electrons/pixel/s. Movies were recorded at 200 ms/frame for 6 s (30 frames), resulting in a total radiation dose of 26.7 electrons/$Å^2$. Defocus range varied between -1.25 µm and -2 µm. For NusA-NusG-TTC-B (n = 12) and NusA-NusG-TTC-LC (n = 12) combined, NusA-NusG-TTC-LC (n = 13), NusA-NusG-TTC-LC (n = 17), NusA-NusG-TTC-LC (n = 20), and NusA-RfaH-TTC-LC (n = 12), datasets of 4,692, 4,544, 4,381, and 5,017 micrographs, respectively, were recorded from single grids over 2-3 days.

Micrographs were gain-normalized and defect-corrected. Data were processed as summarized in Extended Data Figs. 1-3. Data processing was performed using a Tensor TS4 Linux GPU workstation

with four GTX 1080 Ti graphic cards (NVIDIA). Dose-weighting motion correction (3x3 tiles; b-factor = 150) were performed using Motioncor2[43]. Contrast-transfer-function (CTF) estimation was performed using CTFFIND-4.1[44]. Subsequent image processing was performed using Relion 3.0[45]. Automatic particle picking with Laplacian-of-Gaussian filtering yielded initial particle sets for NusA-NusG-TTC-B (n = 12) and NusA-NusG-TTC-LC (n = 12) combined, NusA-NusG-TTC-LC (n = 13), NusA-NusG-TTC-LC (n = 17), NusA-NusG-TTC-LC (n = 20), and NusA-RfaH-TTC-LC (n = 12) of 17,581, 3,213, 122,400, 209,053, and 90,290 particles, respectively. Particles were extracted into 500x500 pixel boxes and subjected to rounds of reference-free 2D classification and removal of poorly populated classes, yielding selected particle sets for NusA-NusG-TTC-B (n = 12), NusA-NusG-TTC-LC (n = 12), NusA-NusG-TTC-LC (n = 13), NusA-NusG-TTC-LC (n = 17), NusA-NusG-TTC-LC (n = 20), and NusA-RfaH-TTC-LC (n = 12) of 3,494, 6,645, 1,516, 24,109, 32,821, and 20,048 particles, respectively,. The resulting selected particle sets were 3D-classified with C1 symmetry, using a *de novo* 3D template created using 3D_initial_model under Relion 3.0. For each complex, classes exhibiting strong, well-defined densities assignable to TEC and ribosome and having a spatial relationship of density for TEC and ribosome consistent with a TTC were combined and were 3D auto-refined using a mask with a diameter of 450 Å. The resulting 3D auto-refined particles were further refined using a soft mask and solvent flattening and were post-processed, yielding reconstructions for NusA-NusG-TTC-B (n = 12), NusA-NusG-TTC-LC (n = 12), NusA-NusG-TTC-LC (n = 13), NusA-NusG-TTC-LC (n = 17), NusA-NusG-TTC-LC (n = 20), and NusA-RfaH-TTC-LC (n = 12) at 6.2, 6.0, 6.2, 3.6, 3.8, and 5.3 Å overall resolution, respectively, as determined from gold-standard Fourier shell correlation (FSC; Extended Data Figs. 1d, 2d, and 3d; Extended Data Tables 1-2). The initial atomic models for TTCs were built as described[33-34]. Refinement of the initial models was performed as described3[3-34]. The initial models were subjected to rounds of manual refinement using Coot[46] and auto-refinement using Phenix real-space refinement[47].

Cryo-EM data for NusA-RfaH-TTC-LC (n = 13) were collected at the Stanford-SLAC Cryo-EM Center, using a 300 kV Titan Krios (FEI/ThermoFisher) electron microscope equipped with a Gatan K3 Quantum

direct electron detector (Gatan) (Extended Data Fig. 3). Data were collected automatically in counting mode using EPU (FEI/ThermoFisher), a nominal magnification of 81,000x, a calibrated pixel size of 0.86 Å/pixel, and a dose rate of 40 electrons/pixel/s. Movies were recorded at 30 ms/frame for 3 s (100 frames), resulting in a total radiation dose of 45 electrons/$Å^2$. Defocus range varied between -0.8 µm and -2.5 µm. A dataset of 7,067 micrographs was recorded from one grid over 2 days. Data were processed as above, yielding a final set of 15,810 particles that produced a reconstruction of 3.4 Å overall resolution (Extended Data Fig. 3d; Extended Data Table 2).

Cryo-EM data for NusG-TTC-X (n = 12), NusG-TTC-X (n = 13), RfaH-TTC-X (n = 12), and RfaH-TTC-X (n = 13) were collected at the Rutgers University Cryo-EM and Nanoimaging Core Facility, as described above and were processed through the 3D auto-refinement stage as described above (Extended Data Figs. 4-5). For NusG-TTC-X (n = 12), NusG-TTC-X (n = 13), RfaH-TTC-X (n = 12), and RfaH-TTC-X (n = 13), datasets of 3,056, 3,763, 4,586, and 8,012 micrographs, respectively, were recorded from single grids over 2-3 days.

Structure visualization was performed using Coot[46], Chimera[48], and PyMOL (Schrödinger).

Final atomic density maps and atomic coordinates for NusA-NusG-TTC-LC (n = 12), NusA-NusG-TTC-LC (n = 13), NusA-NusG-TTC-LC (n = 17), NusA-NusG-TTC-LC (n = 20), NusA-RfaH-TTC-LC (n = 12), and NusA-RfaH-TTC-LC (n = 13) were deposited in the Protein Data Bank and the Electron Microscopy Data Bank with accession codes 8VOP and EMD-43388, 8VOQ and EMD-43389, 8VOR and EMD-43390, 8VOS and EMD-43391, 8VL1 and EMD-43335, and 8VOO and EMD-43387, respectively.

Additional references associated with methods

43. Zheng, S., Palovcak, E., Armache, J., Verba, K., Cheng, Y., and Agard, D. (2017) MotionCor2: anisotropic correction of beam-induced motion for improved cryo-electron microscopy. *Nature Meths.* **14**, 331-333.

44. Rohou, A. and Grigorieff, N. (2015) CTFFIND4: Fast and accurate defocus estimation from electron micrographs. *J. Structl. Biol.* **192**, 216-221.

45. Zivanov, J., Nakane, T., Forsberg, B., Kimanius, D., Hagen, W., Lindahl, E., and Scheres, S. (2018) New tools for automated high-resolution cryo-EM structure determination in RELION-3. Elife **7**, e42166.

46. Emsley, P., Lohkamp, B., Scott, W., and Cowtan, K. (2010) Features and development of Coot. *Acta Cryst. D* **66**, 486-501.

47. Afonine, T., Headd, J., Terwilliger, T. and Adams, P. (2013) Computational Crystallography Newsletter 4, 43-44 (http://phenix-online.org/newsletter/CCN_2013_07.pdf).

48. Pettersen, E., Goddard, T., Huang, C., Couch, G., Greenblatt, D., Meng, E., and Ferrin, T. (2004) UCSF Chimera: a visualization system for exploratory research and analysis. *J. Comp. Chem*. **25**, 1605-1612.

Extended Data Figure Legends

Extended Data Fig. 1. Structure determination: NusA-NusG-TTC-B and NusA-NusG-TTC-LC (n = 12)

(a) Data processing scheme (Extended Data Table 1).

(b) Representative electron micrograph and 2D class averages (100 nm scale bar in left subpanel; 50 nm scale bar in right subpanel).

(c) Orientation distribution.

(d) Fourier-shell-correlation (FSC) plot.

(e) EM density maps colored by local resolution. View orientation as in Figs. 1, 2a, and 2b.

(f) Superimpositions of NusA-NusG-TTC-LC on NusA-NusG-TTC-B subclass B1[32] (left), subclass B2[32] (center), and subclass B3[32] (right).

(g-j) Representative EM densities (blue mesh) and fits (ribbons) for RNAP β' ZBD, ribosomal protein S3, NusG, and NusA.

Extended Data Fig. 2. Structure determination: NusA-NusG-TTC-LC (n = 13, 17, or 20)

(a) Data processing scheme (Extended Data Table 1).

(b) Representative electron micrograph and 2D class averages (100 nm scale bar in left subpanel; 50 nm scale bar in right subpanel).

(c) Orientation distribution.

(d) Fourier-shell-correlation (FSC) plot.

(e) EM density maps colored by local resolution. View orientation as in Figs. 1, 2a, and 2b.

(f) Superimpositions of NusA-NusG-TTC-LC (n = 12, 13, 17, or 20) on NusA-NusG-TTC-B subclass B1[32].

(g-j) Representative EM densities (blue mesh) and fits (ribbons) for RNAP β' ZBD, ribosomal protein S3, NusG, and NusA.

Extended Data Fig. 3. Structure determination: NusA-RfaH-TTC-LC (n = 12 or 13)

(a) Data processing scheme (Extended Data Table 1).

(b) Representative electron micrograph and 2D class averages (100 nm scale bar in left subpanel; 50 nm scale bar in right subpanel).

(c) Orientation distribution.

(d) Fourier-shell-correlation (FSC) plot.

(e) EM density maps colored by local resolution. View orientation as in Figs. 1, 2a, and 2b.

(f) Superimpositions of NusA-RfaH-TTC-LC (n = 12 or 13) on NusA-RfaH-TTC-B[33].

(g-j) Representative EM densities (blue mesh) and fits (ribbons) for RNAP β' ZBD, ribosomal protein S3, RfaH, and NusA.

Extended Data Fig. 4. Structure determination: NusG-coupled TTC containing long mRNA spacer in absence of NusA (NusG-TTC-X; n = 12 or 13)

(a) Data processing scheme.

(b) Representative electron micrograph and 2D class averages (100 nm scale bar in left subpanel; 50 nm scale bar in right subpanel).

(c) Orientation distribution.

(d) Fourier-shell-correlation (FSC) plot.

(e) EM density maps colored by local resolution. View orientation as in Figs. 1, 2a, and 2b.

(f) Superimpositions of NusG-TTC-X (n = 12 or 13) on NusA-NusG-TTC-LC (n = 12).

Extended Data Fig. 5. Structure determination: RfaH-coupled TTC containing long mRNA spacer in absence of NusA (RfaH-TTC-X; n = 12 or 13)

(a) Data processing scheme.

(b) Representative electron micrograph and 2D class averages (100 nm scale bar in left subpanel; 50 nm scale bar in right subpanel).

(c) Orientation distribution.

(d) Fourier-shell-correlation (FSC) plot.

(e) EM density maps colored by local resolution. View orientation as in Figs. 1, 2a, and 2b.

(f) Superimpositions of RfaH-TTC-X (n = 12 or 13) on NusA-RfaH-TTC-LC (n = 12).

Extended Data Fig. 6. Structural modelling: compatibility of TTC-LC with formation of pause and termination RNA hairpins and incompatibility of TTC-LC with engagment of termination factor Rho

(a) TTC-LC (gray) is fully compatible with formation of pause and termination RNA hairpins[39-41] (red; no steric clash).

(b) TTC-LC (gray) is incompatible with egagement of termination factor Rho[24] (cyan with bound mRNA segments in red; severe steric clash with ribosome).

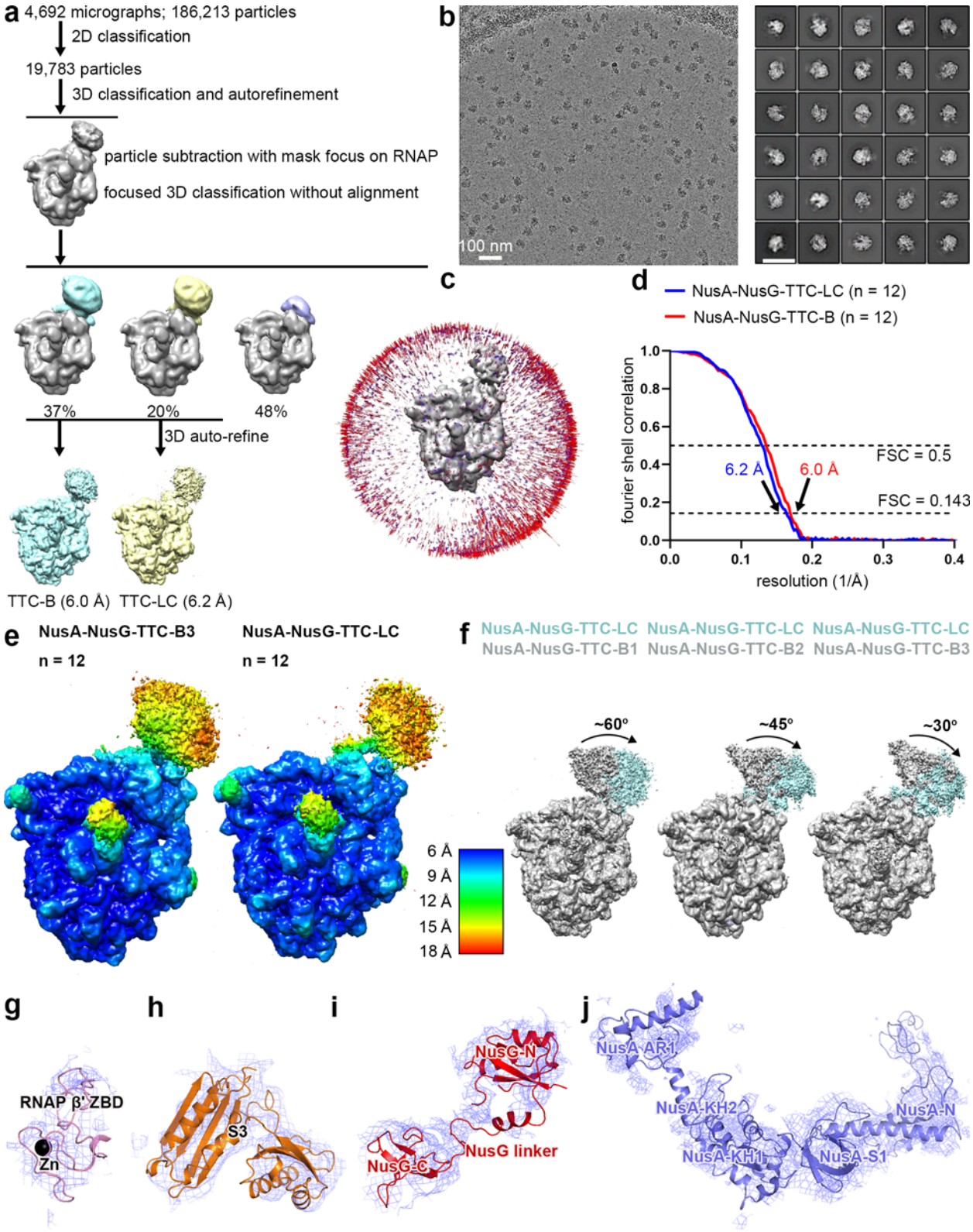

Extended Data Figure 1

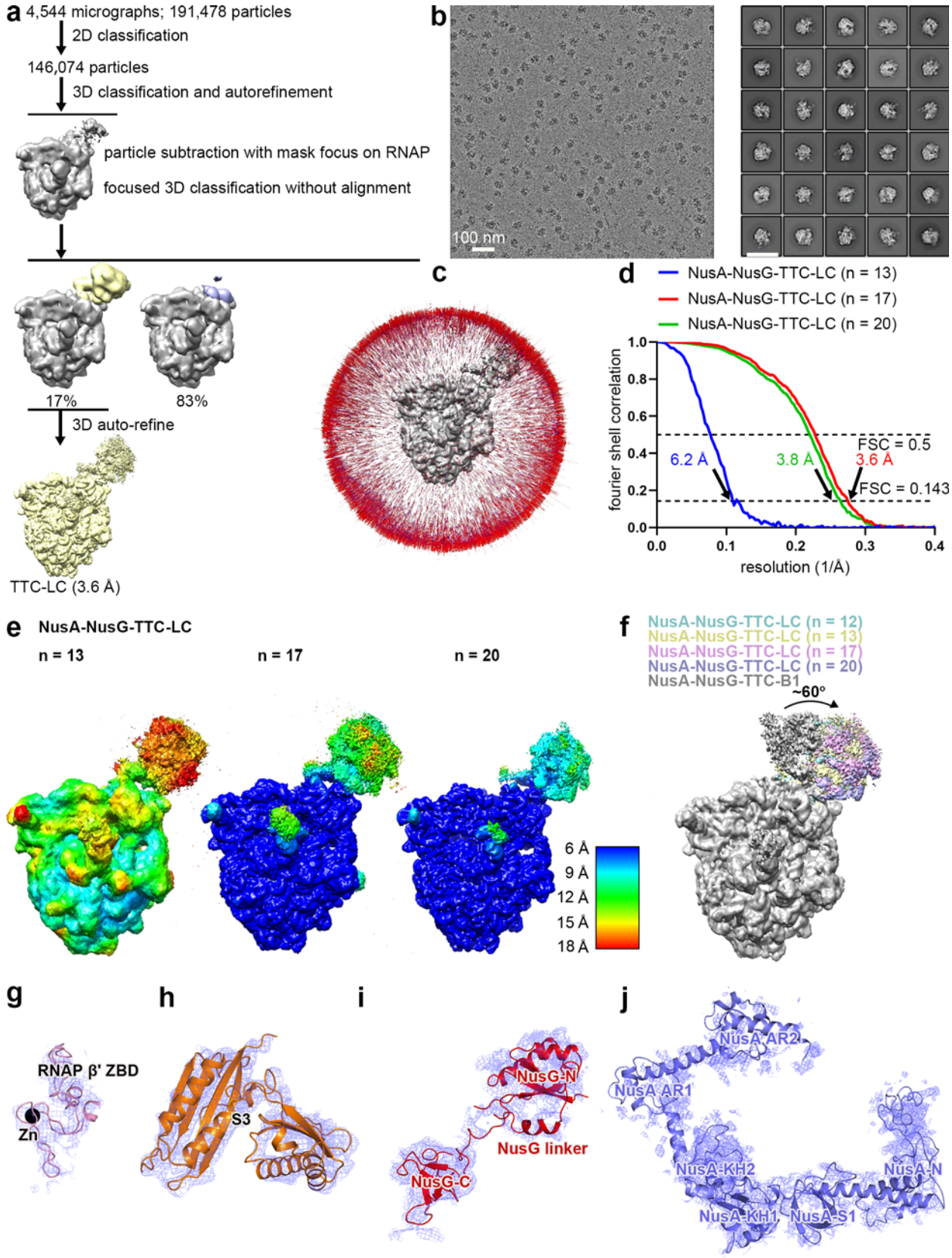

Extended Data Figure 2

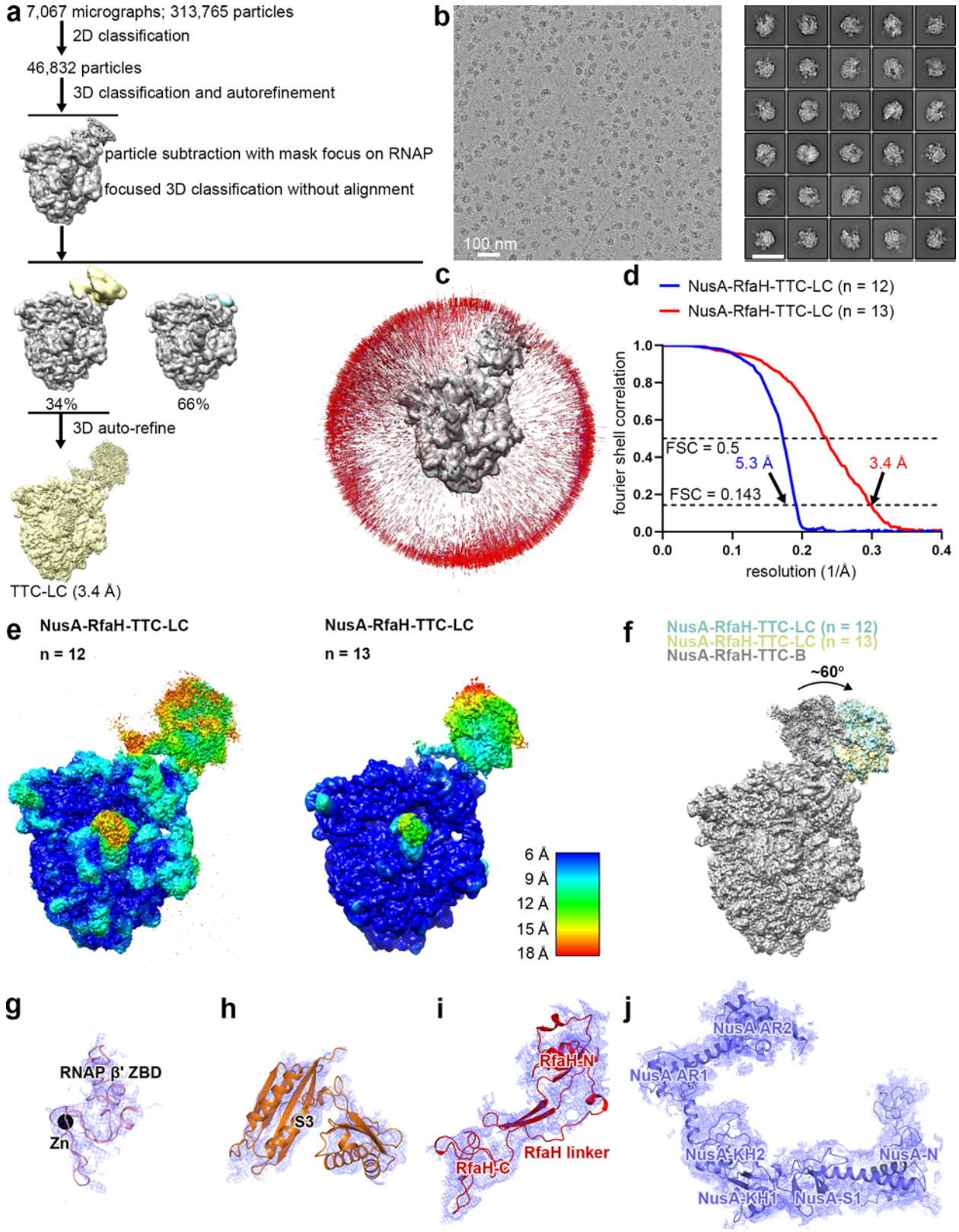

Extended Data Figure 3

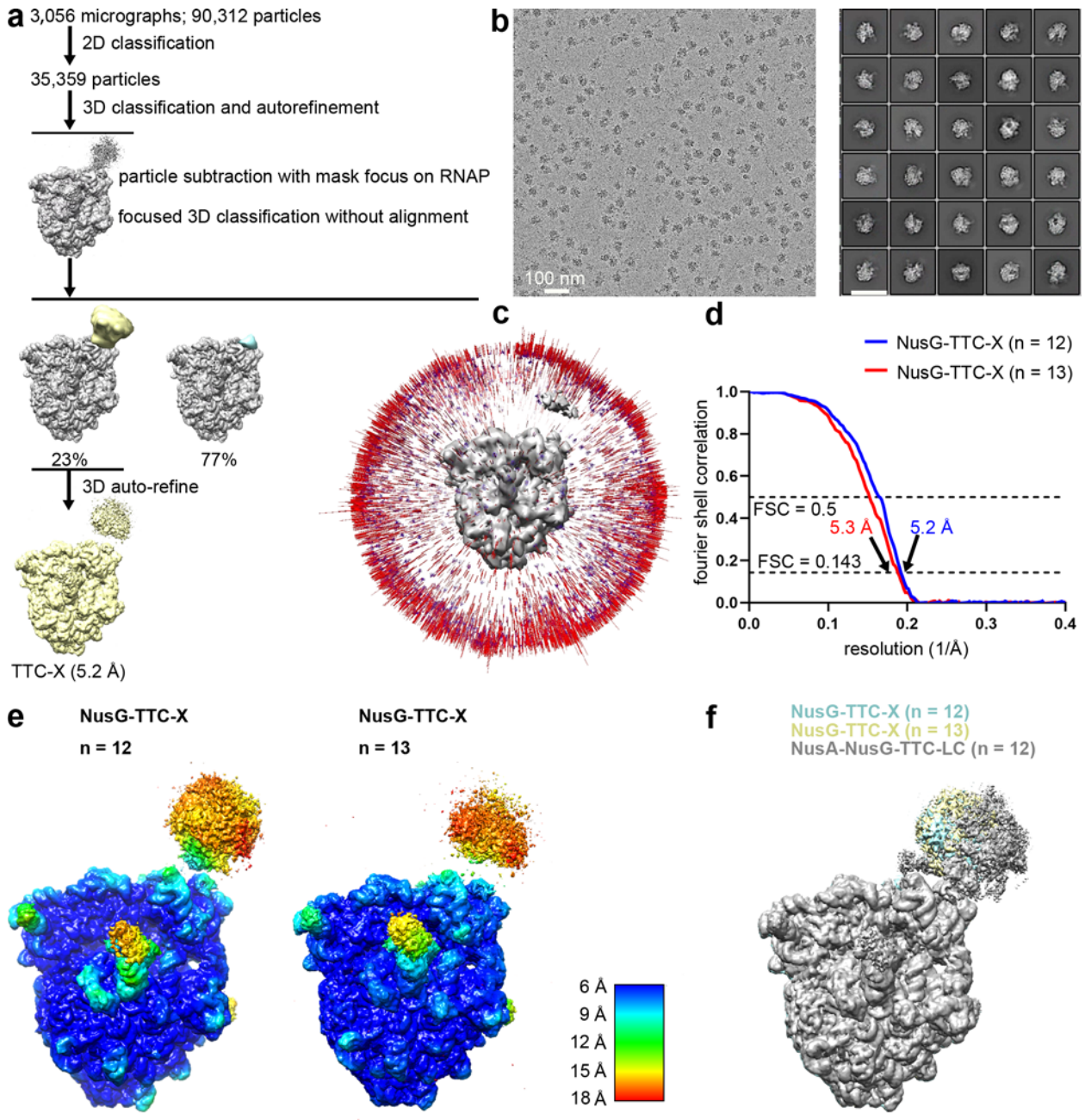

Extended Data Figure 4

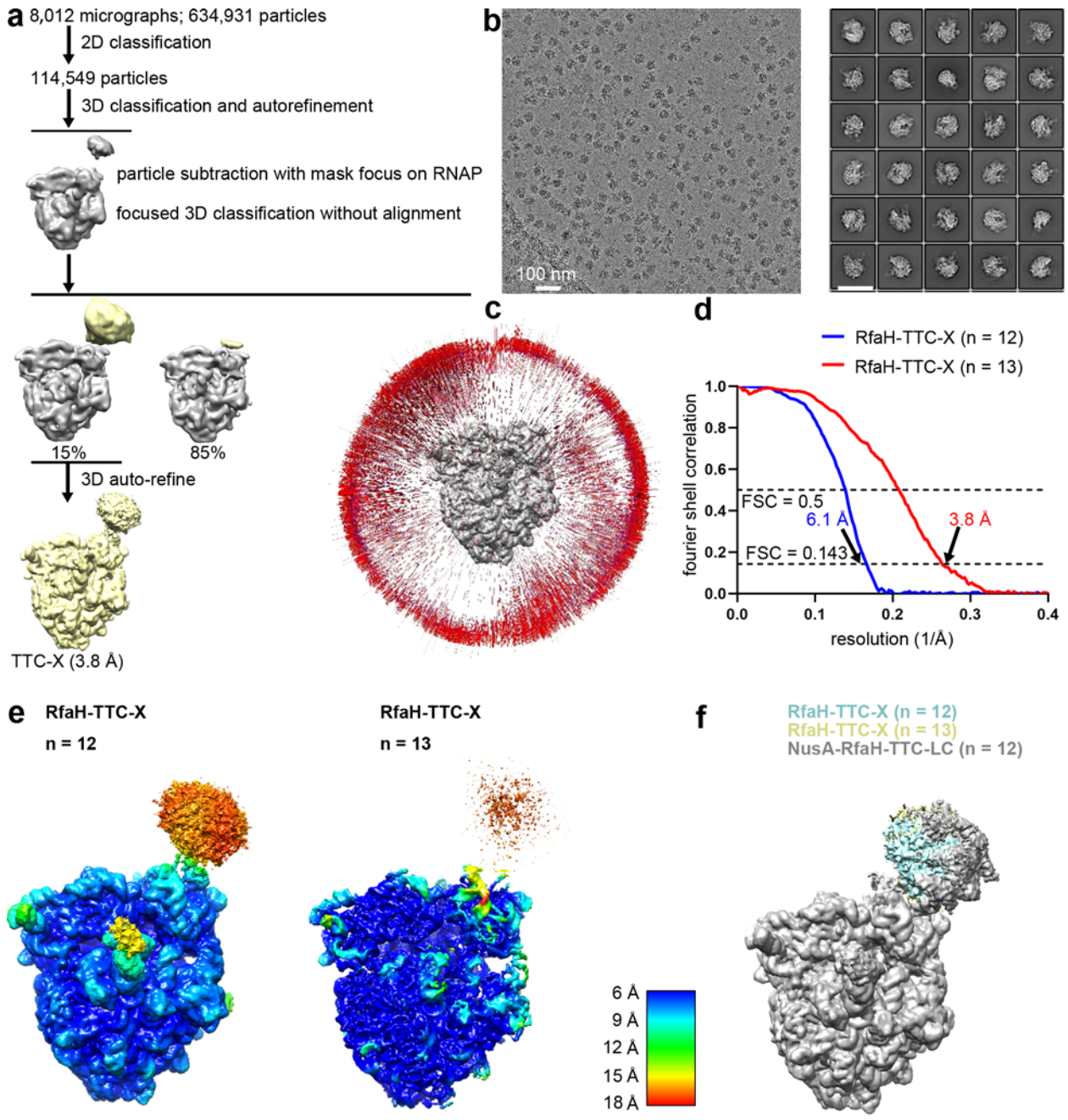

Extended Data Figure 5

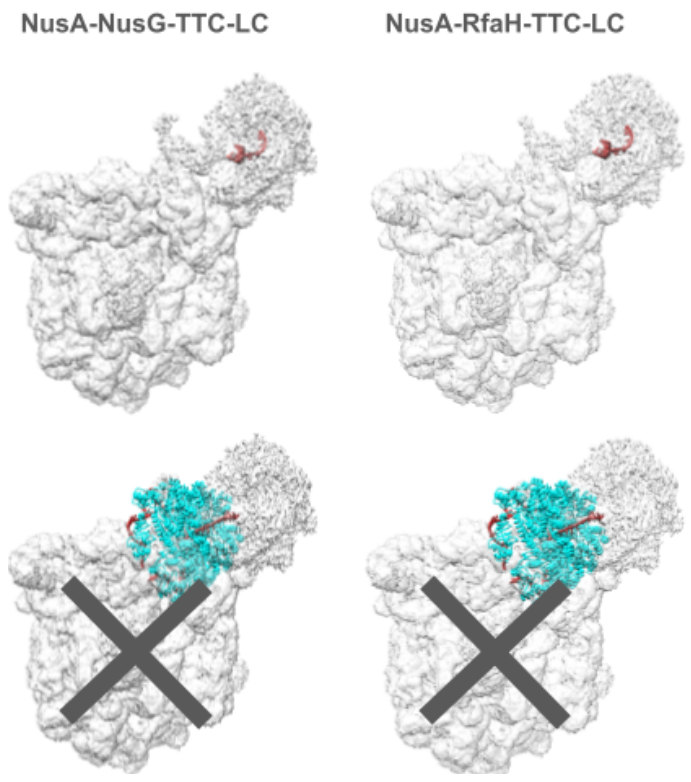

Extended Data Figure 6

Extended Data Table 1: Cryo-EM structures: NusA-NusG-TTC-B (n = 12) and NusA-NusG-TTC-LC (n = 12, 13, 17, and 20)

	NusA-NusG-TTC-B n = 12	**NusA-NusG-TTC-LC n = 12 (EMDB-43388) (PDB 8VOP)**	**NusA-NusG-TTC-LC n = 13 (EMDB-43389) (PDB 8VOQ)**	**NusA-NusG-TTC-LC n = 17 (EMDB-43390) (PDB 8VOR)**	**NusA-NusG-TTC-LC n = 20 (EMDB-43391) (PDB 8VOS)**
Data collection and processing					
Magnification	130,000x	130,000x	130,000x	130,000x	130,000x
Voltage (kV)	200	200	200	200	200
Electron exposure (e–/Å2)	28	28	28	28	28
Defocus range (μm)	-1.25 to -2.0	-1.25 to -2.0	-1.25 to -2.0	-1.25 to -2.0	-1.25 to -2.0
Pixel size (Å)	1.038	1.038	1.038	1.038	1.038
Symmetry imposed	C1	C1	C1	C1	C1
Initial particle images (no.)	1,7581	1,7581	3,213	122,400	209,053
Final particle images (no.)	3,494	6,645	1,516	24,109	32,821
Map resolution (Å)	6.2	6.0	6.2	3.6	3.8
FSC threshold	0.143	0.143	0.143	0.143	0.143
Map resolution range (Å)	5.0-50	5.49-50	6.13-50	3.27-44.37	3.29-50
Refinement					
Initial models used (PDB codes)	6X6T	6X6T	6X6T	6X6T	6X6T
Model resolution (Å)	6.3	6.6	6.8	5.8	6.0

Extended Data Table 2: Cryo-EM structures: NusA-RfaH-TTC-LC (n = 12 and 13)

	NusA-RfaH-TTC-LC n = 12 (EMDB-43335) (PDB 8VL1)	**NusA-RfaH-TTC-LC n = 13 (EMDB-43387) (PDB 8VOO)**
Data collection and processing		
Magnification	130,000x	81,000
Voltage (kV)	200	300
Electron exposure (e–/Å2)	28	45
Defocus range (μm)	-1.25 to -2.0	-1.25 to -2.5
Pixel size (Å)	1.038	0.86
Symmetry imposed	C1	C1
Initial particle images (no.)	90,290	38,467
Final particle images (no.)	20,048	15,810
Map resolution (Å)	5.3	3.4
FSC threshold	0.143	0.143
Map resolution range (Å)	4.89-50	3.21-50
Refinement		
Initial models used (PDB codes)	6C6S, 6X6T	6C6S, 6X6T
Model resolution (Å)	6.8	5.8